

PAPER

iEEGview: an open-source multifunction GUI-based Matlab toolbox for localization and visualization of human intracranial electrodes

To cite this article: Guangye Li *et al* 2020 *J. Neural Eng.* **17** 016016

View the [article online](#) for updates and enhancements.

You may also like

- [Empirical models of scalp-EEG responses using non-concurrent intracranial responses](#)

Komalpreet Kaur, Jerry J Shih and Dean J Krusinski

- [Phase-amplitude coupling between low-frequency scalp EEG and high-frequency intracranial EEG during working memory task](#)

Huanpeng Ye, Guangye Li, Xinjun Sheng et al.

- [Electrical brain stimulation and continuous behavioral state tracking in ambulatory humans](#)

Filip Mivalt, Vaclav Kremen, Vladimir Sladky et al.

Journal of Neural Engineering



PAPER

RECEIVED
4 August 2019

REVISED
15 October 2019

ACCEPTED FOR PUBLICATION
28 October 2019

PUBLISHED
23 December 2019

iEEGview: an open-source multifunction GUI-based Matlab toolbox for localization and visualization of human intracranial electrodes

Guangye Li^{1,4} , Shize Jiang², Chen Chen¹ , Peter Brunner^{3,4}, Zehan Wu², Gerwin Schalk^{3,4}, Liang Chen² and Dingguo Zhang^{5,6}

¹ State Key Laboratory of Mechanical Systems and Vibrations, Institute of Robotics, Shanghai Jiao Tong University, Shanghai, People's Republic of China

² Department of Neurosurgery of Huashan Hospital, Fudan University, Shanghai, People's Republic of China

³ Department of Neurology, Albany Medical College, Albany, NY, United States of America

⁴ National Center for Adaptive Neurotechnologies, Wadsworth Center, New York State Department of Health, Albany, NY, United States of America

⁵ Department of Electronic and Electrical Engineering, University of Bath, Bath, United Kingdom

⁶ Author to whom any correspondence should be addressed.

E-mail: d.zhang@bath.ac.uk

Keywords: localization, visualization, iEEG, SEEG, ECoG, Matlab toolbox, electrodes

Supplementary material for this article is available [online](#)

Abstract

Objective. The precise localization of intracranial electrodes is a fundamental step relevant to the analysis of intracranial electroencephalography (iEEG) recordings in various fields. With the increasing development of iEEG studies in human neuroscience, higher requirements have been posed on the localization process, resulting in urgent demand for more integrated, easy-operation and versatile tools for electrode localization and visualization. With the aim of addressing this need, we develop an easy-to-use and multifunction toolbox called iEEGview, which can be used for the localization and visualization of human intracranial electrodes. **Approach.** iEEGview is written in Matlab scripts and implemented with a GUI. From the GUI, by taking only pre-implant MRI and post-implant CT images as input, users can directly run the full localization pipeline including brain segmentation, image co-registration, electrode reconstruction, anatomical information identification, activation map generation and electrode projection from native brain space into common brain space for group analysis. Additionally, iEEGview implements methods for brain shift correction, visual location inspection on MRI slices and computation of certainty index in anatomical label assignment. **Main results.** All the introduced functions of iEEGview work reliably and successfully, and are tested by images from 28 human subjects implanted with depth and/or subdural electrodes. **Significance.** iEEGview is the first public Matlab GUI-based software for intracranial electrode localization and visualization that holds integrated capabilities together within one pipeline. iEEGview promotes convenience and efficiency for the localization process, provides rich localization information for further analysis and offers solutions for addressing raised technical challenges. Therefore, it can serve as a useful tool in facilitating iEEG studies.

1. Introduction

For patients with medically intractable epilepsy, intracranial electroencephalography (iEEG) has been widely applied in the exploration of the epileptogenic zone and the identification of the eloquent cortex (Behrens *et al* 1994, Lachaux *et al* 2003). In terms of the types of implanted intracranial electrodes,

iEEG mainly includes two modalities. One is known as electrocorticography (ECoG), which implants subdural grid electrodes or strip electrodes and has been the most common technique in the past decades (Crone *et al* 2006). The other modality, named stereoelectroencephalography (SEEG), uses depth electrodes containing multiple contacts to acquire intracranial data, and has become increasingly prevalent in clinical

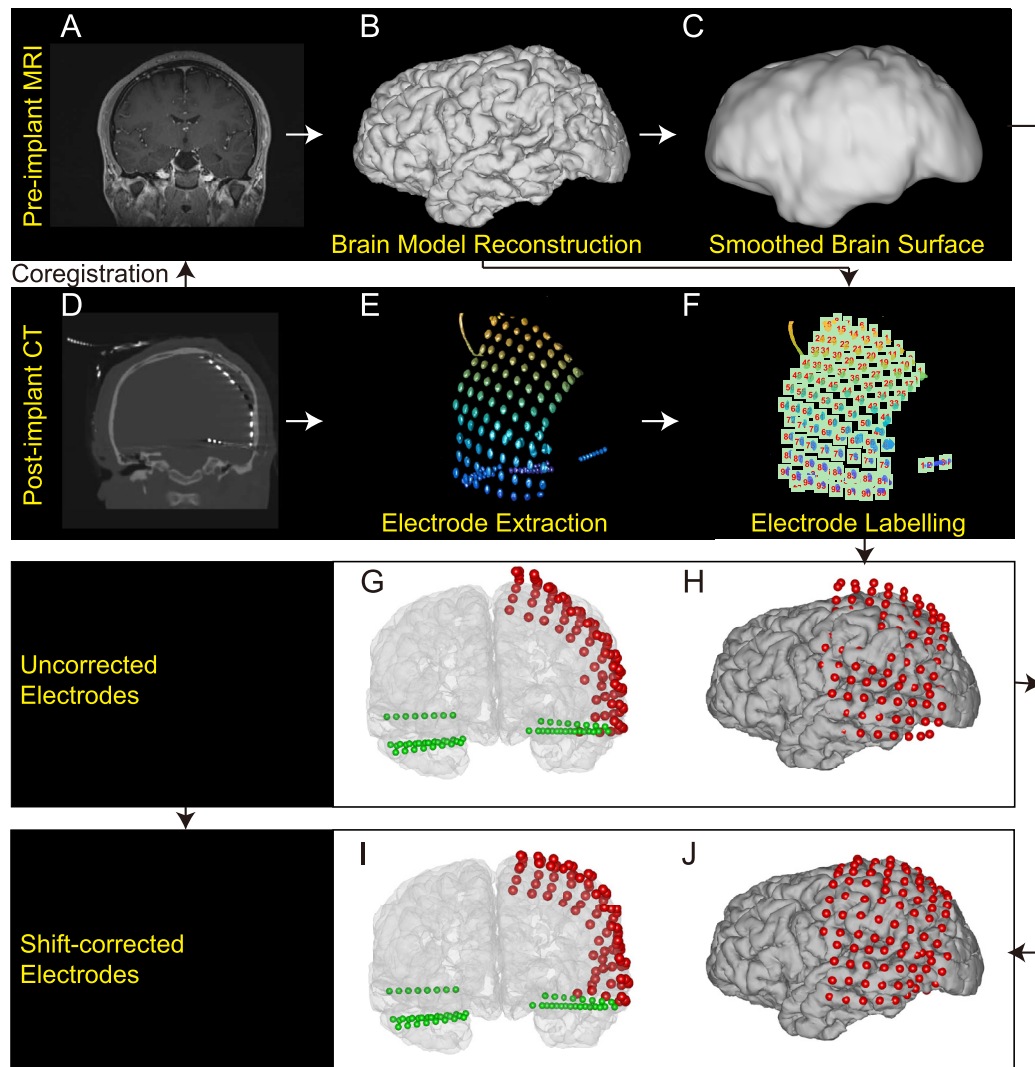


Figure 1. Electrode localization process of the toolbox. (A) Pre-implant MRI images from a single subject. (B) Brain reconstruction results using the MRI images from (A). The brain segmentation results are generated after brain reconstruction. (C) The smoothed brain surface generated after (B). This process is implemented automatically by executing Freesurfer functions from the toolbox. (D) Post-implant CT images are aligned to the MRI images by running the coregistration function from the toolbox. (E) Locations and profiles of all implanted electrodes are extracted from the coregistered CT images. (F) Electrode labelling process after electrode extraction. Coordinates of all the electrodes are computed and transformed into the space where the individual brain (B), (C) is located after this step in the toolbox. (G)/(H) Original reconstructed brain surface and electrodes before brain shift correction. (I)/(J) Reconstructed brain surface and electrodes after brain shift correction. Subject information from Subject 28 is used here for illustration.

practice (Ayoubian *et al* 2010, Cardinale *et al* 2016, Bartolomei *et al* 2018, Britton 2018, Landre *et al* 2018). Owing to its merits of high spatiotemporal resolution and simultaneous recordings across different cortical areas or subcortical structures, iEEG has not only been used for clinical practice but has also become an invaluable tool for neuroscientific research and translational applications (Leuthardt *et al* 2004, Parvizi and Kastner 2018, Ter Wal *et al* 2018).

Notably, accurate localization of intracranial electrodes plays a critical role in guaranteeing the precision of iEEG-related analyses (Pieters *et al* 2013, Taimouri *et al* 2014, Gonzalez-Martinez *et al* 2014). In clinical

practice, accurate information on both the relative position and anatomical location of each iEEG electrode in relation to the brain are extremely important in both the assessment of epileptogenic zone resection (Koessler *et al* 2010, Taimouri *et al* 2014, Trebuchon and Chauvel 2016) and the mapping of the functional cortex (Brunner *et al* 2009, Swift *et al* 2018), while neuroscientific research needs the anatomical label of each iEEG electrode for functional analyses within an individual brain (Coon and Schalk 2016, Schalk *et al* 2017a, Li *et al* 2018a) or the normalized electrode positions across different subjects for group analyses in a standard brain (Posner *et al* 2014, Avanzini *et al*

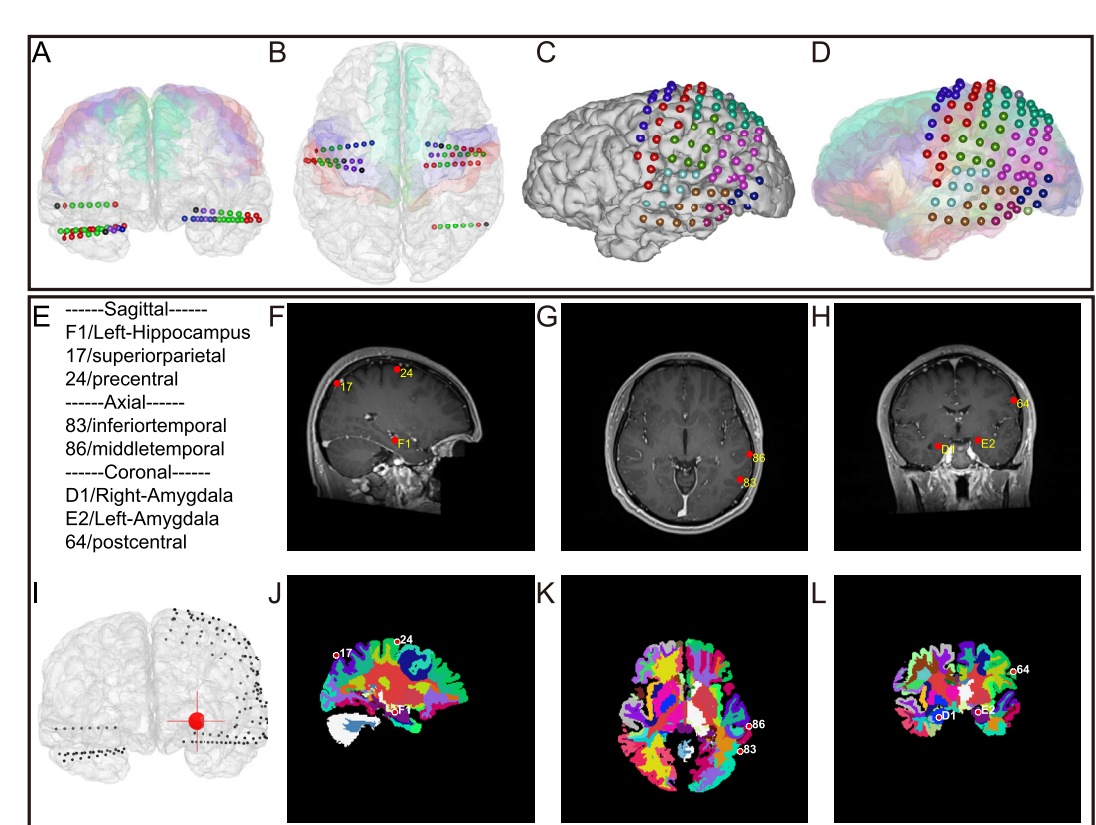


Figure 2. Illustration of the anatomical information identification function of the toolbox. (A)/(B) Coronal/axial view of identified anatomical information for depth electrodes and individual brain. Depth electrode contacts are colored differently to represent different anatomical locations: red for gray matter, green for white matter, purple for hippocampus, blue for amygdala, and black for unknown areas. The different colors on the cortical surface indicate different cortical regions. The toolbox enables the coloring of specified cortical regions based on needs. (C)/(D) Illustration of anatomical identification for subdural electrodes without/with presenting cortical parcellation results (colorful cortex). Anatomical location for each electrode is shown in the same color as the segmented cortical region where the electrode is located. For (A)–(D), the Desikan–Killiany atlas is used here for visualization purposes. (E)–(L) Graphical user interface (GUI) of iEEGview for the manual inspection of each electrode’s anatomical location. Bars used for adjusting image slices are not shown in this figure for visualization purposes. See supplementary materials for more details. (E) Automatically identified anatomical name of electrodes presented in (F)–(H). (F)/(G)/(H) Sagittal/axial/coronal view of electrodes and original MRI images. Electrodes are shown in red dots for each MRI slice if there exists. The name of each electrode is presented in yellow. (I) 3D view of the brain and electrodes. Red cross indicates the real-time coordinates of current image slices. (J)/(K)/(L) Sagittal/axial/coronal view of electrodes and brain segmentation. Electrodes are shown as red dots for each atlas slice if present. Different colors in each slice represent different segmented brain regions. The name of each electrode is shown in white. White matter segmentation results are presented in the images as well. Subject information from Subject 28 are used here for illustration.

2016, Schalk *et al* 2017b, Nourski *et al* 2018, Arnal *et al* 2019, Betzel *et al* 2019). In translational applications (e.g. brain-machine interfaces), identifying the anatomical location of activated electrodes and visualizing the overall subsequent cortical activation map is essential for a better understanding of brain functions during a certain task (Kubanek *et al* 2009, Schalk *et al* 2007, Murphy *et al* 2016, Li *et al* 2017). In summary, to meet the various requirements from existing iEEG applications, the localization process should provide at least four functions, including: (1) localizing the 3D coordinates of iEEG electrodes within each individual brain; (2) identifying the anatomical information for iEEG electrodes for that brain; (3) visualizing brain activation using iEEG recordings; and (4) mapping electrodes from different individual subjects into a standard brain.

Until now, different methods have been developed to locate implanted electrodes. Some methods use solely MRI images to identify electrode locations

(Kovalev *et al* 2005, Yang *et al* 2012); however, the post-implant MRI requires a special type of electrode and also has the potential risk of electrode induction heating (Bhavaraju *et al* 2002). Another method to localize the electrodes is solely through x-ray images (Miller *et al* 2007); although it is time-efficient and comparatively safe, this approach lacks the individual anatomical information. Therefore, the most commonly used method is combining pre-implant MRI and post-implant CT images to obtain greater localization accuracy (van Rooijen *et al* 2013). Although some public software has succeeded in reconstructing iEEG electrode positions using co-registered CT and MRI images (Dykstra *et al* 2012, Taimouri *et al* 2014, Blennemann *et al* 2017), they are short of some important required functions (e.g. visualizing brain activation, identifying anatomical information for each electrode and/or projecting into a standard brain). Meanwhile, some other well-developed software has only been validated for the localization of either depth (Princich

et al 2013, Arnulfo *et al* 2015b, Narizzano *et al* 2017, Medina Villalon *et al* 2018) or subdural (Kovalev *et al* 2005, Hermes *et al* 2010, Azarion *et al* 2014, Branco *et al* 2018a, 2018b) electrodes, and it is not adequate for potential clinical needs when the combination of these two types of electrodes are implanted (Surbeck *et al* 2011, Enatsu *et al* 2014). More recently, a toolbox has been introduced that provides enriched functions and is used for localizing both depth and subdural electrodes (Groppe *et al* 2017), but in one aspect, it lacks the provision of enough important anatomical information for each electrode (e.g. the degree of confidence that a depth electrode contact can be assigned to a brain region); in other aspects, it still needs additional efforts in manual operation across multiple third-party software packages, which may increase the burden for inexperienced users during operation.

To address the above issues, by incorporating previously developed software (Kubanek and Schalk 2015, Li *et al* 2018b), in this work we provide a fully upgraded toolbox package that can localize and visualize depth (SEEG) or subdural (ECoG) electrodes (or a combination) with multiple functions in a semi-automatic way. This toolbox integrates all dependent software into one Matlab interface using command lines. In addition, it is graphic user interface (GUI) based and features a rich range of choices, which is both time-saving and user-friendly. With just simple inputs from the user, guided by the GUI, the toolbox performs the full pipeline (from images to all features as mentioned above).

2. Electrode reconstruction

iEEGview is developed using Matlab (Mathwork, Natick, MA), and also uses some Bash scripts for the automatic interaction with Freesurfer (<http://surfer.nmr.mgh.harvard.edu>). Freesurfer is used for basic image processing, brain reconstruction and electrode profile extraction during the electrode localization process, and Freesurfer-produced results are used across the full localization pipeline. The entire toolbox is required to run under a Mac OS system and has been tested with the Mac OS X system and Matlab version (R2017b, v9.3) or higher. Images from 28 human subjects are used for testing the toolbox (3158 depth electrode contacts and 598 subdural electrodes are implanted in total; all subjects gave the informed consent), where 22 subjects are implanted with depth electrodes (Subjects 1–22), five with subdural electrodes (Subjects 23–27), and one (Subject 28, also known as Subject UCI29) with both depth and subdural electrodes (Stolk *et al* 2018).

The electrode localization process is shown in figure 1. In detail, as the first step of electrode localization, iEEGview takes pre-implant T1-weighted MRI images as inputs and then reconstructs the individual brain model by invoking Freesurfer automatically using Bash scripts (figure 1(A)). This process first

transforms the input MRI brain volume into a Free-surface right-anterior-superior (RAS) coordinate space, then runs the brain volume reconstruction. The reconstruction produces not only the pial and white matter surfaces from both hemispheres (figure 1(B)), but also the cortical parcellation (Fischl 2004, Desikan *et al* 2006, Destrieux *et al* 2009) and subcortical segmentation (Fischl *et al* 2002) results. These results are saved by the toolbox and used for the following localization pipeline.

At the second step, the toolbox aligns post-implant CT (figure 1(D)) with pre-implant MRI automatically using the built-in Matlab functions (`spm_coreg`, `spm_reslice`) from SPM 12 (Penny *et al* 2011). More specifically, the coregistration process is implemented through an affine transformation with six degrees of freedom based on the maximization of normalized mutual information (Studholme *et al* 1998, Jenkinson and Smith 2001). This method has shown good performance for the coregistration of CT and MR images (Studholme *et al* 1998, Hermes *et al* 2010, Azarion *et al* 2014). After this, the toolbox automatically displays the coregistered volumes in Freesurfer. This step enables the user to visually check the coregistration results and also extract the electrode information, including the surfaces and locations of implanted electrodes, by thresholding the coregistered CT images (figure 1(E); see also supplementary materials ([stacks.iop.org/JNE/17/016016/mmedia](https://iop.org/JNE/17/016016/mmedia))). Following this step, the toolbox then provides a GUI for users to manually label⁷ each of the derived electrodes in 3D space (visualized by a small number of vertices and triangles in Matlab, figure 1(F)). For the subdural electrodes, the 3D coordinates of all the electrodes, in the same coordinate space as the individual brain model, are automatically obtained after labelling (figure 1(G)). Notably, such 3D space electrode visualization also provides users with additional advantages towards traditional 2D space visualization (Hermes *et al* 2010, Dykstra *et al* 2012) in the detection of overlapping subdural electrode implants (Branco *et al* 2018a). For depth electrodes, considering the fact that a large number of depth electrode contacts are generally used and the size of each contact is much smaller than for typical subdural electrodes, this process is thus difficult and time-consuming. Therefore, to make the electrode localization process more efficient, iEEGview only requires four randomly spaced points to be selected from each extracted electrode shaft surface to conduct a line-fitting process using the least-squares method (Moré 1978, Li *et al* 2018b), where the first point should be selected from the tip of each electrode shaft (deep brain layer). Then, with the user solely inputting the number of contacts along each electrode shaft from the GUI of iEEGview, the 3D coordinates of all the depth contacts can be automatically generated.

⁷ Feedback on the electrodes that have been labelled is provided in the GUI for convenience of operation.

Notably, brain shift occurs due to various factors that include brain swelling, drainage of cerebrospinal fluid, surgical intervention, and deformation following gravity and electrode implantation (Hastreiter *et al* 2004, Dalal *et al* 2008). Roberts *et al* reported a brain displacement of 1 cm on average during craniotomy (Roberts *et al* 1998). Therefore, to guarantee higher localization accuracy, brain shift correction is generally a necessary step in electrode localization when a craniotomy is made. Using the methods introduced in previous work (Yang *et al* 2012, Kubanek and Schalk 2015, Blenkmann *et al* 2017), we provide brain shift correction functions within the iEEGview toolbox for either when subdural electrodes are implanted solely, or when depth electrodes are implanted along with subdural electrodes where a craniotomy is required. Specifically, for subdural electrodes, a smoothed surface (figure 1(C)) that deprives the reconstructed pial surface of sulci is first built by the toolbox using a morphological closing algorithm for the purpose of projection (Schaer *et al* 2008, Yang *et al* 2012). Before the projection, since this brain surface still consists of a large number of vertices and triangles, which is computationally expensive, we then produce a simplified version of the smoothed brain surface by reducing the vertices and triangles to speed up the calculation for both hemispheres. After this, iEEGview projects each electrode ($P_k(x, y, z)$) onto a coordinate ($P'_k(x, y, z)$) of the simplified brain surface. In brief, the procedure first finds all vertices $V_i(x, y, z)$, ($i = 1 \dots N$) of the simplified brain surface within a predefined radius (e.g. 25 mm by default) from the electrode ($P_k(x, y, z)$). Then, the normal vectors of all the triangles touching these vertices are averaged ($\vec{A}(x, y, z)$). Finally, the intersection between the electrode ($P_k(x, y, z)$) and simplified brain surface following the averaged normal vector ($\vec{A}(x, y, z)$) is identified as a projection point ($P'_k(x, y, z)$) (Kubanek and Schalk 2015). This projection point ($P'_k(x, y, z)$) is used as the final coordinates for each subdural electrode ($P_k(x, y, z)$) after brain shift correction (figures 1(H) and (J)).

For the scenario in which depth and subdural electrodes are implanted simultaneously, we additionally correct the brain shift for depth electrodes. This process is implemented by using a weighted displacement field function based on the subdural electrodes' brain shift correction results and the distance to the uncorrected subdural electrodes (Blenkmann *et al* 2017). In detail, the weighted displacement field function (equation (1)) translates the inputs using two Gaussian kernel-based functions, where one (equation (2)) is used to compute the displacement field (Taimouri *et al* 2014), and the other (equation (3)) weights the displacement field with distance, considering the fact that the depth electrodes located in a deeper layer of the brain are less affected by brain deformation than the ones closer to the brain surface (figures 1(G) and (I)).

$$D_j = \frac{\sum_{k=1}^K w_{jk} w'_{jk} D_k}{\sum_{k=1}^K w_{jk}} \quad (1)$$

$$w_{jk} = e^{-\frac{\|P_j - P_k\|}{\sigma_R^2}} \quad (2)$$

$$w'_{jk} = e^{-\frac{\|P'_j - P'_k\|}{\sigma_D^2}} \quad (3)$$

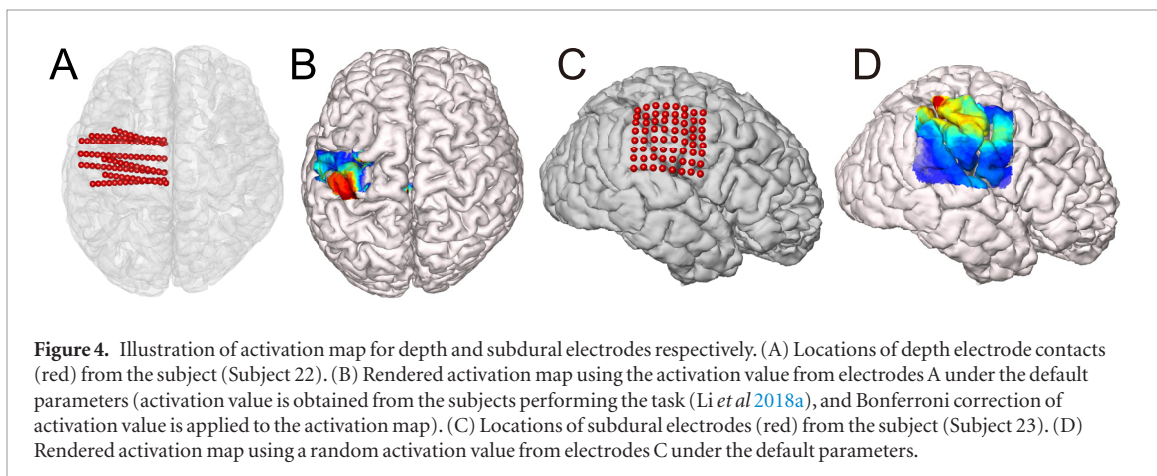
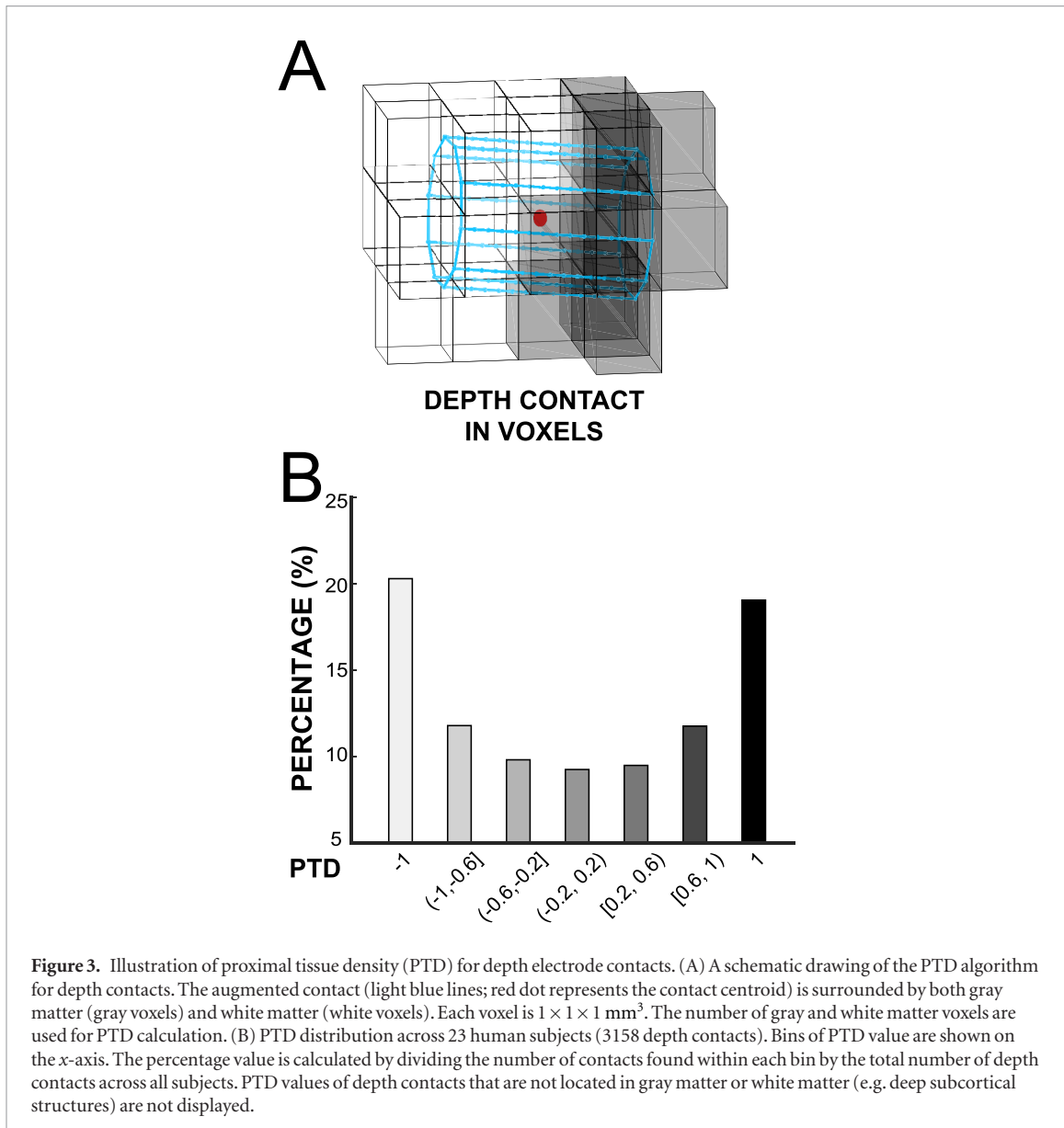
where P_j and P_k are the coordinates of the uncorrected depth contact j and subdural electrode k ; D_k is the projection vector for subdural electrode k ($k = 1 \dots K$), $D_k = P'_k - P_k$; and σ_R and σ_D are regularization parameters and are set as 5 mm and 30 mm within the toolbox, respectively. The final coordinates P'_j for the depth contact P_j after brain shift correction is then obtained as $P'_j = P_j + D_j$.

One of the brain shift correction examples for both subdural and depth electrodes is shown in figures 1(G)–(J). We run this process for each of six applicable subjects, and the averaged brain shift correction value is 3.71 ± 0.13 (mean \pm s.e) mm for subdural electrodes ($n = 568$) and 0.89 ± 0.08 (mean \pm s.e) mm for depth electrode contacts ($n = 32$).

This entire brain and electrode reconstruction process for each subject typically takes about 8–24 h of computing time for brain segmentation from Freesurfer and 30–60 min of operation time (i.e. for localization of all electrodes) for an experienced user.

3. Anatomical information identification

For intracranial electrode-based analysis, another essential requirement is to identify the anatomical location for each electrode. iEEGview automatically identifies the anatomical label for each intracranial electrode (i.e. depth and subdural electrodes) (figure 2). This identification uses the brain segmentation results from Freesurfer (see section 2), which yields a range of different cortical areas and also subcortical structures such as left and right cerebral white matter, caudate, putamen, thalamus, hippocampus, amygdala and other components (Fischl *et al* 2002). The segmentation results are saved in the format of entire brain volume, which is with a size of $256 \times 256 \times 256$ under a voxel-based column–row–slice (CRS) coordinate system. Within the brain volume, each voxel is $1 \times 1 \times 1 \text{ mm}^3$ and carries an anatomical label (figure 3(A)). For depth electrodes (e.g. SEEG), to enhance precision in anatomical label assignment, we use a shape-based volumetric classification method instead of using only the centroid of each contact. More specifically, we build an augmented contact by adding a 0.5 mm tolerance into the original contact (e.g. 2 mm length, 0.8 mm diameter) in both the length and radius direction, and then project this cylinder into the target segmented brain volume. Then we



cluster all the voxels that touch this cylinder, and the anatomical location of the contact is classified into the group that has the maximum number of voxels within this cluster (figures 2(A) and (B)). For subdural electrodes, the anatomical location for each electrode

is identified as the anatomical name of the maximum same-labelled vertex, among the vertices surrounding (e.g. within 5 mm of) the point where the computed electrode is located after brain shift correction (figures 2(C) and (D)). Additionally, to fulfill the multiple

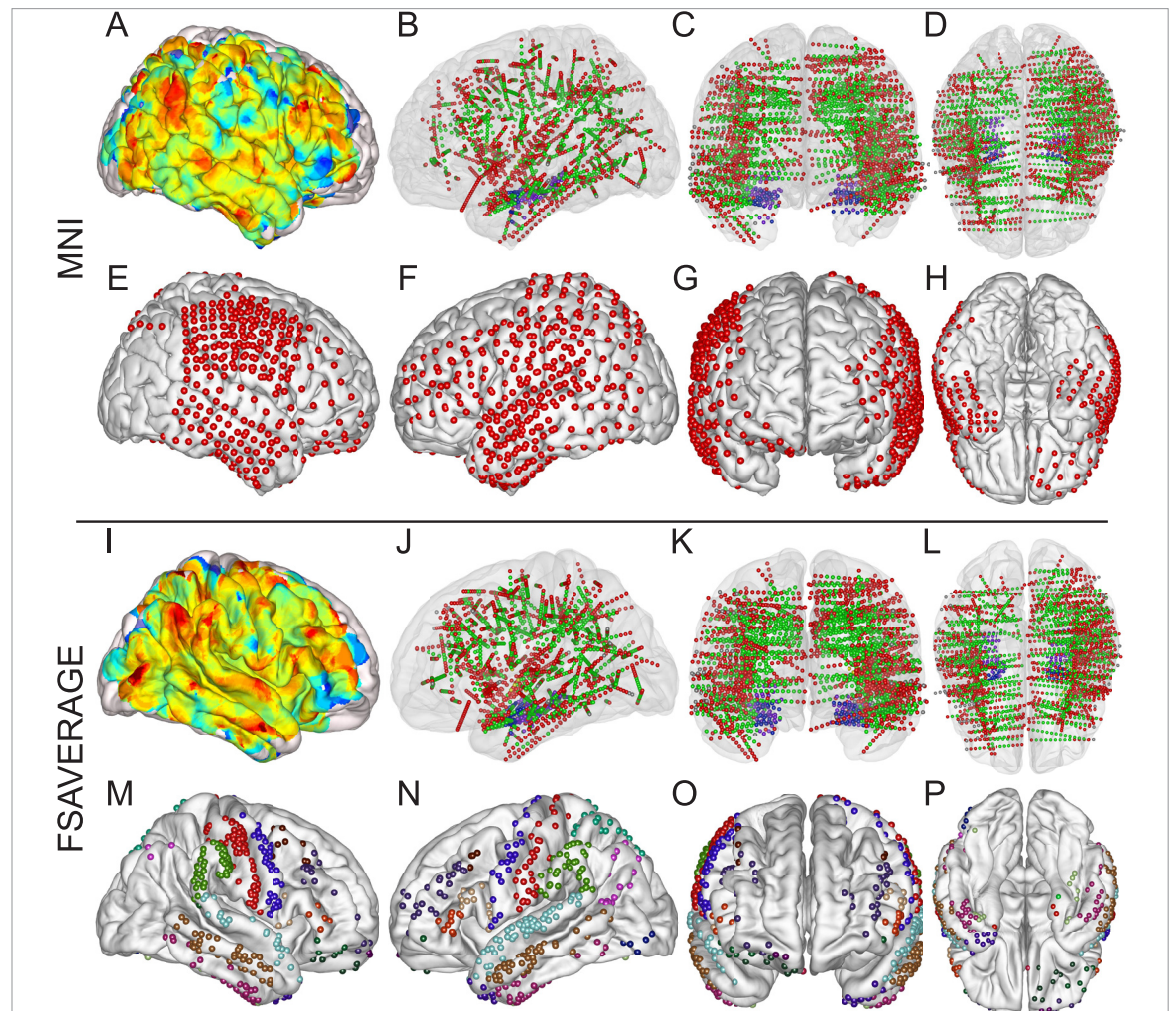


Figure 5. Illustration of mapping into standard brain function for depth electrodes and subdural electrodes. (A) Activation map generated on the Montreal Neurological Institute (MNI) brain model using random activation value from all depth electrodes. All the depth electrodes (B)–(D) are first projected into the right hemisphere for the rendering of the activation map for visualization purposes. (B)/(C)/(D) Sagittal/coronal/axial view of all depth contacts projected into the MNI brain model using the volumetric registration method from 23 subjects (Subjects 1–22 and 28, n = 3158). Contacts are shown by small balls. Different colors represent different anatomical locations, where red indicates gray matter, green indicates white matter, purple indicates hippocampus, blue indicates amygdala, yellow indicates putamen, and gray indicates the remaining regions. (E)/(F)/(G)/(H) Different views of all subdural electrodes projected onto a standard brain model (MNI) from six subjects (Subjects 23–28, n = 568). Each subdural electrode is represented by a red ball. The subdural electrodes from individual subjects are first transformed into the common brain space using volumetric registration method and then projected onto the surface of the MNI brain model (section 2). (I) Activation map generated on the Freesurfer average brain model (FSAverage) using the same activation value as A from all depth electrodes. All the other configurations are the same as A. (J)/(K)/(L) Sagittal/coronal/axial view of all depth contacts projected into the average brain model using linear space transformation from 23 subjects (Subjects 1–22 and 28, n = 3158). All the other configurations are the same as (B)–(D). (F)/(G)/(H) Different views of all subdural electrodes projected onto a standard brain model (FSAverage) using surface-based registration from six subjects (Subjects 23–28, n = 568). Electrodes are shown in different colors based on their anatomical locations. The Desikan–Killiany atlas is used here for visualization purposes.

potential needs, iEEGview provides three atlases (Desikan–Killiany (Desikan *et al* 2006), Destrieux (Fischl 2004, Destrieux *et al* 2009), and DKT40 (Klein and Tourville 2012)) for the identification of cortical areas. Moreover, to meet the possible needs of white-matter-related analysis using depth electrode recordings, the toolbox also provides the function of identifying the anatomical label for the depth electrode contacts located in superficial white matter tracts (tracts of white matter that are closest to divided cortical areas, e.g. pre/post-central white matter, up to 36 zones), where the white matter segmentation results from Freesurfer are used (figures 2(J)–(L)).

Considering that the depth electrode contact is typically a long cylinder shape, therefore, each contact may span two or more different structures (e.g. gray matter and white matter), causing uncertainties in its anatomical location. There are some subcortical studies (e.g. white matter) that may need to find out the contacts that are located in white matter for sure, so as to make the corresponding subcortical analysis robust. For this purpose, iEEGview provides automatic calculation of an index called proximal tissue density (PTD) (Mercier *et al* 2017), which reflects the degree of confidence with which an electrode can be assigned to a particular anatomical region. In detail, for each aug-

mented depth contact, we calculate the PTD following the equation (equation (4)). A schematic drawing of the PTD algorithm is shown in figure 3(A). Using this method, we compute the PTD value across 23 subjects implanted with depth electrodes. The distribution of different PTD value bins is shown in figure 3(B). The results demonstrate that 19.1% of the depth contacts are totally embedded by gray matter, and 20.3% by white matter, leaving approximately 60% of depth contacts surrounded by both gray matter and white matter. These results also emphasize the importance of taking the uncertainty of anatomical labelling into consideration for each depth contact when conducting analysis in relation to anatomy; the introduced PTD index is a feasible solution to this. To enrich the options for the users, we additionally provide the computation of PTD values using the method introduced in (Mercier *et al* 2017), which identifies the number of gray and white matter voxels within a $3 \times 3 \times 3 \text{ mm}^3$ volume surrounding the centroid of each depth contact (equation (4)), where the PTD values computed using both methods are similar (Mercier *et al* 2017):

$$PTD = (V_g - V_w)/(V_g + V_w) \quad (4)$$

where V_g and V_w are the identified number of gray matter and white matter voxels that completely or partially overlap with the contact.

Even though automatically identifying the anatomical location saves time, manual inspection of the anatomical location for each electrode or depth contact is still essential for some experienced users to obtain a higher localization accuracy. Moreover, manual checking also provides more details for the anatomical locations. To fulfill such needs, iEEGview offers the function for manual visual inspection as well. Using this function, the toolbox provides three different views (sagittal, coronal and axial) of both grayscale MRI images and colored segmented brain images. Within each view, the users can visually check the location of each electrode (or depth contact) by simply adjusting the slices of each view (figures 2(F)–(H) and (J)–(L)). In addition, a 3D view of the entire brain and electrodes with a cursor is displayed to show the present slice position for reference (figure 2(I)). The automatically identified anatomical label for the electrodes located in the present MRI slices are shown as well for comparison purposes (figure 2(E); see supplementary materials for more details about the manipulation).

4. Activation map visualization

Visualization of brain topographies associated with neural activity on the cortical surface plays an important role in vividly and directly expressing neural information; we termed it as the activation map here. By giving the activation value, iEEGview can plot the activation map automatically. The activation value can be either a component related to neural activation status (e.g. gamma/alpha activity (Miller *et al* 2010, de

Pesters *et al* 2016)) or a statistical indicator of neural recordings (e.g. $-\log(p)$ value (Schalk *et al* 2007, Li *et al* 2017)). In detail, this process treats each subdural electrode or depth electrode contact as a neural source, where the source is of the same coordinates as the electrode or contact itself after brain shift correction (figures 4(A) and (C); see section 2). iEEGview then computes the effective activation value of each vertex surrounding the electrode (Kubanek and Schalk 2015). This process is made up of four steps: (1) The process first finds all vertices within a certain distance range from the electrode; (2) For each identified vertex, the toolbox provides two different applicable kernel functions (equations (5)–(8)) to calculate the activation factor (K_{act} , [0, 1]) based on the distance from the vertex to the electrode, considering the potential attenuation effect from a neural source; (3) Since one vertex may be affected by multiple sources and hence generate more than one activation factors for each vertex after step 2, the toolbox then implements a normalization procedure to prevent cumulative effects on the following activation value calculation due to differences in number of sources (i.e. dividing K_{act} of each source by the sum of K_{act} from all available sources in each vertex). The activation value of each vertex is computed by multiplying each normalized activation factor by the activation value from each electrode entered by the user; (4) Finally, the activation map is rendered using the averaged activation value carried by each vertex.

Linear Kernel:

$$K_{act}(d) = f_l(d, D) \quad (5)$$

$$f_l(d, D) = \begin{cases} 0; & (d \geq D) \\ 1 - \frac{d}{D}; & (d < D) \end{cases}. \quad (6)$$

Gaussian Kernel:

$$K_{act}(d) = f_g(d, D) \quad (7)$$

$$f_g(d, D) = e^{-\frac{d^2}{2D^2}} \quad (8)$$

where d means the distance from each subdural electrode or depth contact to each cortical vertex within range R (R is adjustable, 10 and 15 mm for subdural and depth electrodes by default in the toolbox), and D is the cutoff distance that is used to adjust the attenuation effect for the activation map (D is adjustable, 10 mm by default in the toolbox).

Within iEEGview, the toolbox provides users with the function of freely choosing and setting the parameters based on personal needs. Examples of rendered activation maps for depth and subdural electrodes are shown in figures 4(B) and (D), respectively.

5. Standard brain mapping

Group level analysis and visualization is always essential in iEEG-based research for uncovering the

universal phenomena underlying the recorded neural activities when studying a large number of subjects. To address the needs for group analysis and visualization, iEEGview provides the function of mapping the intracranial electrodes to a standard brain model across multiple subjects (figure 5).

Specifically, two representative standard brain templates for this function are utilized in the toolbox. One is the Montreal Neurological Institute (MNI) brain template (figures 5(A)–(H)); this brain model is first constructed with high-resolution MRI images from a single subject and thus features rich cortical surface information (known as ‘Colin27’) (Holmes *et al* 1998), and then the template is normalized to MNI152 space in this work (Mazziotta *et al* 1995, Evans *et al* 2012). The other one is the averaged brain from Freesurfer (known as ‘FSAverage’, figures 5(I)–(P), MNI305 space); this brain template is made from the spherical alignment of 40 subjects and features less cortical surface area because each individual’s brain is smoothed out during the group average process (Fischl *et al* 1999).

For subdural electrodes, iEEGview provides two different methods for the mapping of electrodes into the common brain space (Stolk *et al* 2018): volume-based registration (Ashburner and Friston 1999, Fischl *et al* 1999, Conner *et al* 2014) and surface-based registration (Dykstra *et al* 2012). These two different methods are implemented on two brain templates separately. For the volume-based registration method, iEEGview takes the MNI brain template. Specifically, this process first normalizes (`spm_normalise`) the individual brain model to a standard MNI brain template (Mazziotta *et al* 1995), consequently generating the volume registration correspondence between these two brain models, which is represented by a series of nonlinear transformation matrices. Then the process warps all the electrodes from the native brain space into the common MNI brain space (MNI152) using derived nonlinear transformation parameters. For the surface-based registration method, the iEEGview uses the Freesurfer average brain template (FSAverage). Briefly, for each individual brain pial surface, a sphere-version surface is first gyrally aligned to the average brain pial surface (Freesurfer), where the spherical surface has a one-to-one vertex correspondence with the pial surface. Then the toolbox obtains a projection point for each electrode by finding the closest vertex on the pial surface of each individual brain. After this, each projection point on the individual spherical surface is assigned to the nearest vertex on the average brain spherical surface, where the corresponding coordinates of this assigned vertex on the Freesurfer average brain pial surface (FSAverage) are finally identified as the mapping point in the common brain space. For the depth electrodes, iEEGview also provides two different ways of mapping (Stolk *et al* 2018, Li *et al*

2018b) on the two introduced brain templates. One is volume-based registration; this process maps each depth electrode contact into the common MNI brain space (MNI152) nonlinearly, which is the same as with subdural electrodes. The other approach utilizes linear space transformation, which directly projects each depth electrode contact from native brain space to another common brain space (MNI305) where the Freesurfer average brain template is located using an affine transformation (Collins *et al* 1994).

Figure 5 presents the results of introduced standard brain mapping functions using iEEGview for depth and subdural electrodes, where 3158 depth contacts from 23 subjects (Subjects 1–22 and 28) and 568 subdural electrodes from six subjects (Subjects 23–27 and 28) are used. Furthermore, after the mapping, by treating the standard brain as an individual model, iEEGview can compute the group-level activation map directly on the standard brain model using the introduced method (sections 2 and 4) across multiple subjects (figures 5(A) and (I)).

6. Discussion

With the increasing importance of iEEG-related research, public software packages that can address the technical challenges posed in this work are in urgent demand. Here we introduce the iEEGview toolbox for the research community, which meets the criteria of accurate localization of either depth or subdural electrodes, or both. In particular, a GUI with a rich range of choices is developed for iEEGview to implement all the required functions (see supplementary materials), making user operation easy and time-efficient. From the GUI, the user can directly run the full pipeline through the listed menu, starting from pre-implant MRI and post-implant CT images, to the segmentation of the brain, coregistration of images and acquisition of 3D coordinates of all electrodes, to the identification of each electrode’s corresponding anatomical information and visual inspection of each localized electrode on the original MRI slices, to the projection of electrodes from native brain space into a common brain space across multiple subjects, and finally to the computation and visualization of an activation map on the rendered brain surface in both native and common brain space. Additionally, the GUI presents 2D and 3D views of the computing results together on the rendered brain to facilitate the understanding of electrode information in relation to brain anatomy. Importantly, all of these introduced functions have been validated successfully across a large number of subjects ($n = 28$).

Brain shift correction for subdural and depth electrodes is implemented in iEEGview when subdural electrodes are implanted solely or together with depth electrodes, where a craniotomy is made. The mean

correction distance achieved from multiple subjects using methods proposed in this work (section 2) is comparable with previous studies (Hermes *et al* 2010, Dykstra *et al* 2012, Blenkmann *et al* 2017, Branco *et al* 2018a), certifying the localization accuracy of the current toolbox. In contrast, when only depth electrodes are implanted, we do not implement such a correction because the brain shift caused in stereotactic surgeries is generally small (Elias *et al* 2007, Sweet *et al* 2013). This is the same as in other studies (Arnulfo *et al* 2015b, Narizzano *et al* 2017, Medina Villalon *et al* 2018).

Notably, iEEG has been extensively adopted for studying the human cortex layer over the past few decades (Schalk *et al* 2007, Coon *et al* 2016, Swift *et al* 2018). Subcortical structures, such as white matter, remain largely ignored and unknown. Meanwhile, depth electrodes have huge potential to be taken as a unique tool to investigate signals recorded under gray matter with high temporal resolution (Parvizi and Kastner 2018). However, these studies rely on accurate identification of the anatomical location of each depth electrode contact. iEEGview has the capability to fulfill such needs in several aspects. First, the iEEGview toolbox can identify the anatomical information for each depth electrode contact and provide various atlases for users to choose from. Second, for the channels located in superficial white matter fiber tracts (Guevara *et al* 2017), iEEGview can also provide the labels of cortical regions of interest (ROIs) that these white matter channels are adjacent to based on the Freesurfer white matter segmentation results (Salat *et al* 2009). Third, the toolbox provides a measure of the degree of confidence with which an electrode can be assigned to a particular anatomical region (e.g. PTD), which is essential in the evaluation of subcortical structures (Arnulfo *et al* 2015a, Mercier *et al* 2017). Just recently, a toolbox developed for estimating the probability of intracranial electrodes being assigned to a specific neuroanatomical atlas using a different approach has been reported (Behncke *et al* 2019), indicating again the importance of offering the probability of anatomical label assignment for each electrode in iEEG studies.

In addition to the above features, the toolbox provides the techniques for mapping intracranial electrodes into common brain space using volumetric and/or surface-based registration methods implementing the two most commonly used brain templates. In detail, both volumetric (Conner *et al* 2014, Schalk *et al* 2017b) and surface-based (Dykstra *et al* 2012, Groppe *et al* 2017) mapping approaches are offered for subdural electrodes; moreover, for depth electrodes, the toolbox also provides volumetric transformation (Blenkmann *et al* 2017, Sani *et al* 2018) and linear space transformation (Groppe *et al* 2017, Li *et al* 2018a) mapping methods. Moreover, iEEGview integrates these mapping techniques for sudural and depth electrodes on the same brain template, and thus, either of these two templates can accommodate both

subdural and depth electrodes together. This design may benefit the user from several aspects: first, it enables the user to analyze directly across different electrode types within one standard brain model without extra transforming efforts between spaces; second, it also provides the possibility to make separate cross-modality comparisons (e.g. fMRI results) for comprehensive brain physiology studies; and third, providing two brain templates could also meet various potential needs of group analysis to a larger extent. Even though we have introduced a series of intersubject mapping techniques, notably, we do not compare mapping accuracy between the proposed methods in this work, since the ability to cross-register functional intracranial recordings across various individuals has proven difficult and thus will be further investigated (Wu *et al* 2018).

Even though iEEGview has provided a set of essential functions for localizing and visualizing intracranial electrodes, there are still some shortcomings of the current software package. One is that we used a manual or semi-automatic method (e.g. labelling each of the subdural electrodes or labelling four points along each depth electrode shaft), instead of a fully automatic detection method, to obtain the coordinates of all electrodes by thresholding the CT images after coregistration. Compared with the automatic approach (Blenkmann *et al* 2017), the current method we have used in iEEGview will be helpful in preventing mistaken detection when the contrast of CT images between the electrodes and brain tissues is not high enough; however, automatic detection would generally be much more time-efficient. Therefore, an automatic detection algorithm for both depth and subdural electrodes should be developed and provided as an option for users in the next stage.

Additionally, as a measure of cortical activities, we provide the function of visualizing the activation map within the current toolbox. One limitation is that the rendered activation map is only at cortical level; however, since the application of depth electrodes, it will be interesting to visualize neural activities from the subcortical regions or structures. By taking advantage of the functions we offered within the toolbox (section 3 and 4), we can also color the subcortical activation areas directly on each corresponding MRI slice for depth electrodes in the future, which will help to produce a 3D neural activity map inside the entire brain volume and may also help to study the functions of different subcortical regions. In addition to the interpolated activation maps, another approach of enriching activation data visualization is plotting electrodes with different activation values (e.g. represented by different electrode diameters or colors), which can give a direct sense of neural activation distribution across the brain volume. In spite of the need to visualize the activation map using a single neuroimaging modality, cross-modality studies also ask for the visualization

of neural activity from multiple neuroimaging data for cross-validation. A function proposed in a recent versatile toolbox, iELVis (Groppe *et al* 2017), presenting multimodal overlay in the same brain, may act as a solution to address this need. In further work, we will add these newly introduced features into the current toolbox to provide users with additional advantages towards visualization for iEEG-related studies.

Additionally, this toolbox has been developed to promote convenience and efficiency of localization, but it still has room for improvement in terms of operation. First, it is currently designed for the Mac operating system, and thus this may restrict wider usage of the toolbox. Therefore, making it compatible with more operating systems in the next step is necessary in order to serve the scientific community more widely. Second, during the visual inspection of anatomical labels for each electrode (section 3), we provide the operation on 2D slices under three different views instead of manipulating in 3D view directly. Although 2D-view operation can fulfill basic needs, providing the function of manipulation in 3D view is generally more intrinsic and convenient for users during operation (Blenkmann *et al* 2017, Branco *et al* 2018a). Third, Freesurfer is used in this toolbox. Even though we have integrated the dependent third-party software into one Matlab interface using command lines, developing a toolbox that is fully independent from any third-party software will add significant convenience for users and thus deserves to be tried in the future.

Finally, iEEGview provides functions mainly for intracranial electrode localization and visualization, while as another aspect of iEEG studies, signal processing and analysis of iEEG recordings is also of considerable importance. To address this need, some public software packages, such as EEGLAB (Delorme and Makeig 2004), Brainstorm (Tadel *et al* 2011), Fieldtrip (Oostenveld *et al* 2011) and eConnectome (He *et al* 2011) provide plentiful and useful functions for processing and analysis of electrophysiological data. For the iEEGview package, once the localization of electrodes is completed, with the proper processing of recorded signals, it is easily extensible for visualizing purposes of certain iEEG-related studies, such as epileptic seizure onset detection (Bartolomei *et al* 2008), functional mapping (Brunner *et al* 2009, Trebuchon and Chauvel 2016) and 3D brain connectivity network (Brovelli *et al* 2017, Ter Wal *et al* 2018). Hence, to better serve the research and clinical community, it is worth the effort of building an additional signal processing and analyzing module in the future. The authors also welcome field researchers to make contributions to this software together.

7. Conclusions

In the present work, we introduce a multifunction toolbox, iEEGview, for the localization and visualization of human intracranial electrodes. To our

best knowledge, iEEGview is the first public Matlab toolbox that integrates the introduced prominent features together, including: (1) localizing depth and subdural electrodes (or a combination) with brain shift correction; (2) identifying the anatomical label of each electrode, providing an additional visual inspection function and computing degree of confidence in assigning an anatomical label for each depth electrode contact; (3) supporting activation map generation; (4) offering methods for mapping two types of electrodes (i.e. depth and subdural) from native into common brain space; (5) providing GUI-based operation, from where users can run the full localization pipeline with low dependence on third-party software. In summary, iEEGview holds integrated capabilities for intracranial electrode localization and visualization, offers simplicity and reliability in terms of operation, and provides solutions for addressing technical challenges that have been raised in this field. Consequently, iEEGview may serve as an effective and practical tool in promoting human iEEG studies.

Acknowledgments

This work was supported by grants from the National Natural Science Foundation of China (No. 91848112, No. 61761166006), the Shanghai Municipal Commission of Health and Family Planning (No. 2017ZZ01006), the Natural Science Foundation and Major Basic Research Program of Shanghai (No. 16JC1420102), and the Shanghai Municipal Science and Technology Major Project (No. 2018SHZDZX03). The software package is freely available through the link (<https://github.com/GuangyeLiGit/iEEGview.git>).

Appendix A. Abbreviations

Alphabetical list of abbreviations used in this paper.

CRS	Column–row–slice
CT	Computerized tomography
ECoG	Electrocorticography
fMRI	Functional magnetic resonance imaging
GUI	Graphical user interface
iEEG	Intracranial electroencephalography
MNI	Montreal Neurological Institute
MRI	Magnetic resonance imaging
PTD	Proximal tissue density
RAS	Right-anterior-superior
ROI	Region of interest
SEEG	Stereo-electroencephalography
SPM	Statistical parametric mapping

Appendix B. Supplementary material

A demonstration video of iEEGview is attached in this section.

ORCID iDs

Guangye Li  <https://orcid.org/0000-0003-2530-3916>
Chen Chen  <https://orcid.org/0000-0002-3007-4364>

References

- Arnal L H, Kleinschmidt A, Spinelli L, Giraud A L and Megevand P 2019 The rough sound of salience enhances aversion through neural synchronisation *Nat. Commun.* **10** 3671
- Arnulfo G, Hirvonen J, Nobili L, Palva S and Palva J M 2015 Phase and amplitude correlations in resting-state activity in human stereotactical EEG recordings *NeuroImage* **112** 114–27
- Arnulfo G, Narizzano M, Cardinale F, Fato M M and Palva J M 2015 Automatic segmentation of deep intracerebral electrodes in computed tomography scans *BMC Bioinform.* **16** 99
- Ashburner J and Friston K J 1999 Nonlinear spatial normalization using basis functions *Hum. Brain Mapp.* **7** 254–66
- Avanzini P, Abdollahi R O, Sartori I, Caruana F, Pelliccia V, Casaceli G, Mai R, Lo Russo G, Rizzolatti G and Orban G A 2016 Four-dimensional maps of the human somatosensory system *Proc. Natl Acad. Sci. USA* **113** E1936–43
- Ayoubian L, Lacoma H and Gotman J 2010 Automatic seizure detection in SEEG using high frequency activities in wavelet domain *Med. Eng. Phys.* **35** 319–28
- Azarian A A et al 2014 An open-source automated platform for three-dimensional visualization of subdural electrodes using CT-MRI coregistration *Epilepsia* **55** 2028–37
- Bartolomei F, Chauvel P and Wendling F 2008 Epileptogenicity of brain structures in human temporal lobe epilepsy: a quantified study from intracerebral EEG *Brain* **131** 1818–30
- Bartolomei F, Nica A, Valenti-Hirsch M P, Adam C and Denuelle M 2018 Interpretation of SEEG recordings *Neurophysiol. Clin.* **48** 53–7
- Behncke J, Kern M, Ruescher J, Schulze-Bonhage A and Ball T 2019 Probabilistic neuroanatomical assignment of intracranial electrodes using the ELAS toolbox *J. Neurosci. Methods* **327** 108396
- Behrens E, Zentner J, van Roost D, Hufnagel A, Elger C E and Schramm J 1994 Subdural and depth electrodes in the presurgical evaluation of epilepsy *Acta Neurochir.* **128** 84–7
- Betzel R F, Medaglia J D, Kahn A E, Soffer J, Schonhaut D R and Bassett D S 2019 Structural, geometric and genetic factors predict interregional brain connectivity patterns probed by electrocorticography *Nat. Biomed. Eng.* **3** 902–16
- Bhavaraju N C, Nagaraddi V, Chetlapalli S R and Osorio I 2002 Electrical and thermal behavior of non-ferrous noble metal electrodes exposed to MRI fields *Magn. Reson. Imaging* **20** 351–7
- Blenkemann A O, Phillips H N, Princich J P, Rowe J B, Bekinschtein T A, Muravchik C H and Kochen S 2017 iElectrodes: a comprehensive open-source toolbox for depth and subdural grid electrode localization *Frontiers Neuroinform.* **11** 14
- Branco M P, Gaglianese A, Glen D R, Hermes D, Saad Z S, Petridou N and Ramsey N F 2018 ALICE: a tool for automatic localization of intra-cranial electrodes for clinical and high-density grids *J. Neurosci. Methods* **301** 43–51
- Branco M P, Leibbrandt M, Vansteensel M J, Freudenburg Z V and Ramsey N F 2018 GridLoc: an automatic and unsupervised localization method for high-density ECoG grids *NeuroImage* **179** 225–34
- Britton J W 2018 Electrical stimulation mapping with stereo-EEG electrodes *J. Clin. Neurophysiol.* **35** 110–4
- Brovelli A, Badier J M, Bonini F, Bartolomei F, Coulon O and Auzias G 2017 Dynamic reconfiguration of visuomotor-related functional connectivity networks *J. Neurosci.* **37** 839–53
- Brunner P et al 2009 A practical procedure for real-time functional mapping of eloquent cortex using electrocorticographic signals in humans *Epilepsy Behav.* **15** 278–86
- Cardinale F, Gonzalez-Martinez J and Lo Russo G 2016 SEEG, happy anniversary! *World Neurosurg.* **85** 1–2
- Collins D L, Neelin P, Peters T M and Evans A C 1994 Automatic 3D intersubject registration of MR volumetric data in standardized Talairach space *J. Comput. Assist. Tomogr.* **18** 192–205
- Conner C R, Chen G, Pieters T A and Tandon N 2014 Category specific spatial dissociations of parallel processes underlying visual naming *Cereb. Cortex* **24** 2741–50
- Coon W G and Schalk G 2016 A method to establish the spatiotemporal evolution of task-related cortical activity from electrocorticographic signals in single trials *J. Neurosci. Methods* **271** 76–85
- Coon W G, Gunduz A, Brunner P, Ritaccio A L, Pesaran B and Schalk G 2016 Oscillatory phase modulates the timing of neuronal activations and resulting behavior *NeuroImage* **133** 294–301
- Crone N E, Sinai A and Korzeniewska A 2006 *High-Frequency Gamma Oscillations and Human Brain Mapping with Electrocorticography* vol 159 (Amsterdam: Elsevier) pp 275–95
- Dalal S S, Edwards E, Kirsch H E, Barbaro N M, Knight R T and Nagarajan S S 2008 Localization of neurosurgically implanted electrodes via photograph–MRI–radiograph coregistration *J. Neurosci. Methods* **174** 106–15
- de Pesters A et al 2016 Alpha power indexes task-related networks on large and small scales: a multimodal ECoG study in humans and a non-human primate *NeuroImage* **134** 122–31
- Delorme A and Makeig S 2004 EEGLAB: an open source toolbox for analysis of single-trial EEG dynamics including independent component analysis *J. Neurosci. Methods* **134** 9–21
- Desikan R S et al 2006 An automated labeling system for subdividing the human cerebral cortex on MRI scans into gyral based regions of interest *NeuroImage* **31** 968–80
- Destrieux C, Fischl B, Dale A M and Halgren E 2009 A sulcal depth-based anatomical parcellation of the cerebral cortex *NeuroImage* **47** S151
- Dykstra A R, Chan A M, Quinn B T, Zepeda R, Keller C J, Cormier J, Madsen J R, Eskandar E N and Cash S S 2012 Individualized localization and cortical surface-based registration of intracranial electrodes *NeuroImage* **59** 3563–70
- Elias W J, Fu K M and Frysinger R C 2007 Cortical and subcortical brain shift during stereotactic procedures *J. Neurosurg.* **107** 983–8
- Enatsu R, Bulacio J, Najm I, Wyllie E, So N K, Nair D R, Foldvary-Schaefer N, Bingaman W and Gonzalez-Martinez J 2014 Combining stereo-electroencephalography and subdural electrodes in the diagnosis and treatment of medically intractable epilepsy *J. Clin. Neurosci.* **21** 1441–5
- Evans A C, Janke A L, Collins D L and Baillet S 2012 Brain templates and atlases *NeuroImage* **62** 911–22
- Fischl B 2004 Automatically parcellating the human cerebral cortex *Cereb. Cortex* **14** 11–22
- Fischl B et al 2002 Whole brain segmentation *Neuron* **33** 341–55
- Fischl B, Sereno M I, Tootell R B and Dale A M 1999 High-resolution intersubject averaging and a coordinate system for the cortical surface *Hum. Brain Mapp.* **8** 272–84
- Gonzalez-Martinez J, Mullin J, Vadera S, Bulacio J, Hughes G, Jones S, Enatsu R and Najm I 2014 Stereotactic placement of depth electrodes in medically intractable epilepsy *J. Neurosurg.* **120** 639–44
- Groppe D M, Bickel S, Dykstra A R, Wang X, Megevand P, Mercier M R, Lado F A, Mehta A D and Honey C J 2017 iELVis: an open source MATLAB toolbox for localizing and visualizing human intracranial electrode data *J. Neurosci. Methods* **281** 40–8
- Guevara M, Roman C, Houenou J, Duclap D, Poupon C, Mangin J F and Guevara P 2017 Reproducibility of superficial white matter tracts using diffusion-weighted imaging tractography *NeuroImage* **147** 703–25
- Hastreiter P, Rezk-Salama C, Soza G, Bauer M, Greiner G, Fahlbusch R, Ganslandt O and Niemsky C 2004 Strategies for brain shift evaluation *Med. Image Anal.* **8** 447–64

- He B, Dai Y, Astolfi L, Babiloni F, Yuan H and Yang L 2011 eConnectome: a Matlab toolbox for mapping and imaging of brain functional connectivity *J. Neurosci. Methods* **195** 261–9
- Hermes D, Miller K J, Noordmans H J, Vansteensel M J and Ramsey N F 2010 Automated electrocorticographic electrode localization on individually rendered brain surfaces *J. Neurosci. Methods* **185** 293–8
- Holmes C J, Hoge R, Collins L, Woods R, Toga A W and Evans A C 1998 Enhancement of MR images using registration for signal averaging *J. Comput. Assist. Tomogr.* **22** 324–33
- Jenkinson M and Smith S 2001 A global optimisation method for robust affine registration of brain images *Med. Image Anal.* **5** 143–56
- Klein A and Tourville J 2012 101 labeled brain images and a consistent human cortical labeling protocol *Frontiers Neurosci.* **6** 171
- Koessler L, Benar C, Maillard L, Badier J M, Vignal J P, Bartolomei F, Chauvel P and Gavaret M 2010 Source localization of ictal epileptic activity investigated by high resolution EEG and validated by SEEG *NeuroImage* **51** 642–53
- Kovalev D, Spreer J, Honegger J, Zentner J, Schulze-Bonhage A and Huppertz H J 2005 Rapid and fully automated visualization of subdural electrodes in the presurgical evaluation of epilepsy patients *Am. J. Neuroradiol.* **26** 1078
- Kubanek J and Schalk G 2015 NeuralAct: a tool to visualize electrocortical (ECOG) activity on a three-dimensional model of the cortex *Neuroinformatics* **13** 167–74
- Kubanek J, Miller K J, Ojemann J G, Wolpaw J R and Schalk G 2009 Decoding flexion of individual fingers using electrocorticographic signals in humans *J. Neural Eng.* **6** 066001
- Lachaux J P, Rudrauf D and Kahane P 2003 Intracranial EEG and human brain mapping *J. Physiol.-Paris* **97** 613–28
- Landre E, Chipaux M, Maillard L, Szurhaj W and Trebuchon A 2018 Electrophysiological technical procedures *Neurophysiol. Clin.* **48** 47–52
- Leuthardt E C, Schalk G, Wolpaw J R, Ojemann J G and Moran D W 2004 A brain-computer interface using electrocorticographic signals in humans *J. Neural Eng.* **1** 63–71
- Li G, Jiang S, Paraskevopoulos S E, Wang M, Xu Y, Wu Z, Chen L, Zhang D and Schalk G 2018 Optimal referencing for stereo-electroencephalographic (SEEG) recordings *NeuroImage* **183** 327–35
- Li G, Jiang S, Wang M, Wu Z, Brunner P, Schalk G, Chen L and Zhang D 2018 SEEGview: a toolbox for localization and visualization of stereo-electroencephalography (SEEG) electrodes *2018 IEEE Int. Conf. on Systems, Man, and Cybernetics (SMC)* 67–70
- Li G, Jiang S, Xu Y, Wu Z, Chen L and Zhang D 2017 A preliminary study towards prosthetic hand control using human stereo-electroencephalography (SEEG) signals *2017 8th Int. IEEE/EMBS Conf. on Neural Engineering (NER)* 375–8
- Mazziotta J C, Toga A W, Evans A, Fox P and Lancaster J 1995 A probabilistic atlas of the human brain: theory and rationale for its development *NeuroImage* **2** 89–101
- Medina Villalon S, Paz R, Roehri N, Lagarde S, Pizzo F, Colombet B, Bartolomei F, Carron R and Benar C G 2018 EpiTools, a software suite for presurgical brain mapping in epilepsy: Intracerebral EEG *J. Neurosci. Methods* **303** 7–15
- Mercier M R, Bickel S, Megevand P, Groppe D M, Schroeder C E, Mehta A D and Lado F A 2017 Evaluation of cortical local field potential diffusion in stereotactic electro-encephalography recordings: a glimpse on white matter signal *NeuroImage* **147** 219–32
- Miller K J, Makeig S, Hebb A O, Rao R P N, den Nijs M and Ojemann J G 2007 Cortical electrode localization from x-rays and simple mapping for electrocorticographic research: the ‘location on cortex’ (LOC) package for MATLAB *J. Neurosci. Methods* **162** 303–8
- Miller K J, Schalk G, Fetz E E, den Nijs M, Ojemann J G and Rao R P N 2010 Cortical activity during motor execution, motor imagery, and imagery-based online feedback *Proc. Natl Acad. Sci. USA* **107** 4430
- Moré J J 1978 *The Levenberg–Marquardt Algorithm: Implementation and Theory* (Berlin: Springer) 105–16
- Murphy B A, Miller J P, Gunalan K and Ajiboye A B 2016 Contributions of subsurface cortical modulations to discrimination of executed and imagined grasp forces through stereoelectroencephalography *PLoS ONE* **11** e0150359
- Narizzano M, Arnulfo G, Ricci S, Toselli B, Tisdall M, Canessa A, Fato M M and Cardinale F 2017 SEEG assistant: a 3DSlicer extension to support epilepsy surgery *BMC Bioinform.* **18** 124
- Nourski K V, Steinschneider M, Rhone A E, Kawasaki H, Howard M A and Banks M I 2018 Processing of auditory novelty across the cortical hierarchy: an intracranial electrophysiology study *NeuroImage* **183** 412–24
- Oostenveld R, Fries P, Maris E and Schoffelen J M 2011 FieldTrip: open source software for advanced analysis of MEG, EEG, and invasive electrophysiological data *Comput. Intell. Neurosci.* **2011** 1
- Parvizi J and Kastner S 2018 Promises and limitations of human intracranial electroencephalography *Nat. Neurosci.* **21** 474–83
- Penny W D, Friston K J, Ashburner J T, Kiebel S J and Nichols T E 2011 *Statistical Parametric Mapping: The Analysis of Functional Brain Images* (Amsterdam: Elsevier)
- Pieters T A, Conner C R and Tandon N 2013 Recursive grid partitioning on a cortical surface model: an optimized technique for the localization of implanted subdural electrodes *J. Neurosurg.* **118** 1086–97
- Posner M, Szczepanski S M, Crone N E, Kuperman R A, Auguste K I, Parvizi J and Knight R T 2014 Dynamic changes in phase-amplitude coupling facilitate spatial attention control in fronto-parietal cortex *PLoS Biology* **12** e1001936
- Princich J P, Wassermann D, Latini F, Oddo S, Blenkmann A O, Seifer G and Kochen S 2013 Rapid and efficient localization of depth electrodes and cortical labeling using free and open source medical software in epilepsy surgery candidates *Frontiers Neurosci.* **7** 260
- Roberts D W, Miga M I, Hartov A, Kennedy F E and Paulsen K D 1998 Intraoperative brain shift and deformation: a quantitative analysis of cortical displacement in 28 cases *Neurosurgery* **43** 749–58
- Salat D H, Lee S Y, van der Kouwe A J, Greve D N, Fischl B and Rosas H D 2009 Age-associated alterations in cortical gray and white matter signal intensity and gray to white matter contrast *NeuroImage* **48** 21–8
- Sani O G, Yang Y, Lee M B, Dawes H E, Chang E F and Shafechi M M 2018 Mood variations decoded from multi-site intracranial human brain activity *Nat. Biotechnol.* **36** 954–61
- Schaer M, Cuadra M B, Tamarit L, Lazeyras F, Eliez S and Thiran J P 2008 A surface-based approach to quantify local cortical gyration *IEEE Trans. Med. Imaging* **27** 161–70
- Schalk G, Kapeller C, Guger C, Ogawa H, Hiroshima S, Lafer-Sousa R, Saygin Z M, Kamada K and Kanwisher N 2017 Facephenes and rainbows: causal evidence for functional and anatomical specificity of face and color processing in the human brain *Proc. Natl Acad. Sci. USA* **114** 12285–90
- Schalk G, Kubanek J, Miller K J, Anderson N R, Leuthardt E C, Ojemann J G, Limbrick D, Moran D, Gerhardt L A and Wolpaw J R 2007 Decoding two-dimensional movement trajectories using electrocorticographic signals in humans *J. Neural Eng.* **4** 264–75
- Schalk G, Marple J, Knight R T and Coon W G 2017 Instantaneous voltage as an alternative to power- and phase-based interpretation of oscillatory brain activity *NeuroImage* **157** 545–54
- Stolk A, Griffin S, van der Meij R, Dewar C, Saez I, Lin JJ, Piantoni G, Schoffelen J M, Knight R T and Oostenveld R 2018 Integrated analysis of anatomical and electrophysiological human intracranial data *Nat. Protocols* **13** 1699–723
- Studholme C, Hawkes D J and Hill D L 1998 Normalized entropy measure for multimodality image alignment *Medical Imaging 1998: Image Processing* vol 3338 pp 132–43
- Surbeck W, Bouthillier A, Weil A G, Crevier L, Carmant L, Lortie A, Major P and Nguyen D K 2011 The combination of subdural and depth electrodes for intracranial EEG investigation of suspected insular (perisylvian) epilepsy *Epilepsia* **52** 458–66

- Sweet J A, Hdeib A M, Sloan A and Miller J P 2013 Depths and grids in brain tumors: implantation strategies, techniques, and complications *Epilepsia* **54** 66–71
- Swift J R, Coon W G, Guger C, Brunner P, Bunch M, Lynch T, Frawley B, Ritaccio A L and Schalk G 2018 Passive functional mapping of receptive language areas using electrocorticographic signals *Clin. Neurophysiol.* **129** 2517–24
- Tadel F, Baillet S, Mosher J C, Pantazis D and Leahy R M 2011 Brainstorm: a user-friendly application for MEG/EEG analysis *Comput. Intell. Neurosci.* **2011** 8
- Taimouri V *et al* 2014 Electrode localization for planning surgical resection of the epileptogenic zone in pediatric epilepsy *Int. J. Comput. Assist. Radiol. Surg.* **9** 91–105
- Ter Wal M, Cardellicchio P, LoRusso G, Pelliccia V, Avanzini P, Orban G A and Tiesinga P H E 2018 Characterization of network structure in stereoEEG data using consensus-based partial coherence *NeuroImage* **179** 385–402
- Trebuchon A and Chauvel P 2016 Electrical stimulation for seizure induction and functional mapping in stereoelectroencephalography *J. Clin. Neurophysiol.* **33** 511–21
- van Rooijen B D, Backes W H, Schijns O E, Colon A and Hofman P A 2013 Brain imaging in chronic epilepsy patients after depth electrode (stereoelectroencephalography) implantation: magnetic resonance imaging or computed tomography? *Neurosurg.* **73** 543–9
- Wu J, Ngo G H, Greve D, Li J, He T, Fischl B, Eickhoff S B and Yeo B T 2018 Accurate nonlinear mapping between MNI volumetric and FreeSurfer surface coordinate systems *Hum. Brain Mapp.* **39** 3793–808
- Yang A I, Wang X, Doyle W K, Halgren E, Carlson C, Belcher T L, Cash S S, Devinsky O and Thesen T 2012 Localization of dense intracranial electrode arrays using magnetic resonance imaging *NeuroImage* **63** 157–65